Journal of The Electrochemical Society

The Electrochemical Society
Advancing solid state & electrochemical science & technology

OPEN ACCESS

Electrochemical Preparation of Cobalt-Samarium Nanoparticles in an Aprotic Ionic Liquid

To cite this article: Marjanul Manjum *et al* 2020 *J. Electrochem. Soc.* **167** 042505

Journal of The Electrochemical Society, 2020 **167** 042505

Electrochemical Preparation of Cobalt-Samarium Nanoparticles in an Aprotic Ionic Liquid

Marjanul Manjum,[1,*] Nobuyuki Serizawa,[1,] Adriana Ispas,[2,**] Andreas Bund,[2,**] and Yasushi Katayama[1,**,z]**

[1]*Department of Applied Chemistry, Faculty of Science and Technology, Keio University, Yokohama, Kanagawa 223-8522, Japan*
[2]*Electrochemistry and Electroplating Group, Technische Universität Ilmenau, Ilmenau D-98693, Germany*

Electrochemical preparation of Co-Sm nanoparticles was conducted in an aprotic room temperature ionic liquid, 1-butyl-1-methylpyrrolidinium bis(trifluoromethylsulfonyl)amide (BMPTFSA) containing $Co(TFSA)_2$ and $Sm(TFSA)_3$. The cyclic voltammetry on a glassy carbon (GC) electrode indicated the electrochemically generated Sm(II) reacted with Co(II) at 25 °C. Potentiostatic cathodic reduction on a GC electrode in BMPTFSA containing 30 mM $Co(TFSA)_2$ and 5 mM $Sm(TFSA)_3$ at 25 °C gave the deposits, which were found to be composed of Co and Sm by energy dispersive X-ray spectroscopy (EDX). The deposits were found to be the aggregates of $SmCo_7$ nanoparticles by transmission electron microscopy (TEM) and X-ray photoelectron spectroscopy (XPS). The formation of $SmCo_7$ nanoparticles dispersed in the ionic liquid was also confirmed by TEM. $SmCo_7$ nanoparticles were considered to form by the disproportionation reaction of Sm(II) in the presence of elementary Co, which was formed by the reduction of Co(II) by Sm(II).

 [DOI: 10.1149/1945-7111/ab79a8]

Manuscript submitted January 13, 2020; revised manuscript received February 6, 2020. Published March 5, 2020.

Magnetic alloy nanoparticles have drawn much attention as attractive materials in magnetic resonance imaging, drug targeting, magnetic refrigeration systems, ferrofluids, and catalysis for their improved magnetic, catalytic, and optical properties.[1–3] Specifically, such rare earth-transition metal (RE-TM) alloy nanoparticles as Co-Sm, Sm-Fe-N, and Nd-Fe-B are well-known for their remarkable magnetic properties, which have wide applications in the field of micro electro mechanical system (MEMS), consumer electronics, automobile, military equipment, and magnetic storage industries.[4–12] Various attempts have been made to prepare magnetic alloy nanoparticles by different methods. However, the reports on the electrochemical preparation of such alloy nanoparticles are limited.[2,3,13] Nowadays, Co-Sm is considered as an important material in MEMS because of its high Curie temperature and excellent thermal stability as compared with Nd-based alloys.[14–17] It has already been revealed the potential to produce nanometer structures with excellent magnetic properties.[12] Although Co-Sm magnets are more expensive than Nd magnets, the electrochemical preparation of Co-Sm nanoparticles may lower the supply risk of Co and/or Sm and environmental issues related with primary mining and ore processing. However, it is also essential to recover the transition metals, rare earth metals, and their alloys and/or nanoparticles from electronic waste to reduce the environmental impact. However, the electrochemical study of rare earth metals has been restricted in aqueous media owing to their negative reduction potentials as compared with those of other metals. RE-TM nanoparticles must be prepared in high temperature molten salts and/or room-temperature ionic liquids because of their wider electrochemical potential windows.[18] Compared with high temperature molten salts, room-temperature ionic liquids are advantageous to the preparation of the nanoparticles due to the ease of handling and no need of energy for heating.

Among room-temperature ionic liquids, pyrrolidinium-based ionic liquid, comprised of 1-butyl-1-methylpyrrolidinium (BMP^+) and bis(trifluromethylsulfonyl)amide ($TFSA^-$), have attracted more attention because of its wide electrochemical potential window and acceptable ionic conductivity. The cation and anion of the room temperature ionic liquid should be selected with caution to prepare RE-TM nanoparticles because the rare-earth nanoparticles are considered to be reactive. The $TFSA^-$-based ionic liquid maintains the stability against moisture and chemical reactivity. Moreover, BMPTFSA is also considered as a crucial medium for stabilizing the nanoparticles without additional organic reagents.[19–27]

Although the electrodeposition of RE-TM alloys from aqueous media is problematic due to the negative reduction potential of the RE elements (more negative than –2.3 V vs SHE), there are various reports on the production of the RE-TM alloys from aqueous media.[28–44] Besides, the preparation of RE-TM alloys from non-aqueous media has been attempted by many researchers.[45–50] For example, Gomez et al. and Cojocaru et al. investigated the electrodeposition of Co-Sm from a deep eutectic solvent (DES) based on choline chloride and urea (1ChCl:2U) at 70 °C. They also discussed the co-deposition of Co and Sm.[51–53] The electrochemical studies on rare earth species, such as Eu(III), Ce(III), Nd(III), Pr(III), Yb(III), and Sm(III), have been reported in various ionic liquids by many researchers.[54–65] Their studies revealed the nature of the rare earth species in different ionic liquids at various temperatures. Some researcher also discussed the electrochemical behavior of rare earth species in ionic liquids containing halide ions such as bromide (Br^-) and chloride ions.[64,65] But, the reports on the electrodeposition of Co-Sm alloy in ionic liquids are limited. Ispas et al. reported the electrochemical behavior of Co and Sm species and the deposition of Co-Sm alloy in BMPTFSA at different temperatures.[55] They discussed the formation of a thin film of Co, Sm, and Co-Sm alloy. Chen et al. studied the deposition of Co-Sm alloy in 1-ethyl-3-methylimidazolium chloride ionic liquid and found Co-Sm crystalline nanowires at a high concentration of Sm speceis.[62] The electrochemical reactions and co-deposition of Co and Sm species were conducted in 1-butyl-3-methylimidazolium tetrafluoroborate by Cui et al.[63] However, in the above studies, the electrochemical reactions between transition metals and rare earth metals as well as the electrochemical formation of RE-TM alloy nanoparticles have not been clarified distinctly.

In our previous reports, electrodeposition of Co was observed in BMPTFSA at 25 °C–200 °C.[66–68] Furthermore, the electrochemical reduction of Sm(III) to Sm(II) at 25 °C and the formation of Sm

*Electrochemical Society Student Member.
**Electrochemical Society Member.
[z]E-mail: katayama@applc.keio.ac.jp

nanoparticles have been investigated in BMPTFSA at 100 °C.[69–71] However, the electrochemical preparation of Co-Sm nanoparticles has not been recognized in BMPTFSA at 25 °C. Although the deposition of Co-Sm alloy was reported in BMPTFSA at different temperatures, the electrochemical reaction between Co and Sm and the formation of Co-Sm nanoparticles with a specific atomic ratio were not discussed in detail.[55]

In the present study, the electrochemical preparation of Co-Sm nanoparticles was explored in BMPTFSA at 25 °C. Furthermore, the reaction between Co and Sm species was also investigated to reveal the reaction mechanism for the formation of Co-Sm nanoparticles in BMPTFSA.

Experimental

The Br^- salt of BMP^+ was prepared by the reaction of 1-methylpyrrolidine (Tokyo Chemical Industry) and butyl bromide (Tokyo Chemical Industry), in acetonitrile (Fujifilm Wako Pure Chemical Corp.) at room temperature, then purified by recrystallization and finally dried under vacuum at 100 °C for 28 h. BMPTFSA was synthesized by interacting BMPBr with LiTFSA (Solvay) in deionized water. The ionic liquid phase was separated by the extraction into dichloromethane (Junsei Chemical) and then finally dried under vacuum at 100 °C for 28 h. The water content in BMPTFSA was found to be less than 1 ppm by Karl Fischer titration (Metrohm, 831 KF Coulometer). $Co(TFSA)_2$ and $Sm(TFSA)_3$ were prepared by the reactions of $CoCO_3$ (Kanto Chemical) and Sm_2O_3 (Fujifilm Wako Pure Chemical Corp.) with HTFSA (Kanto Chemical) at 60 °C and 80 °C, respectively, by the reactions 1 and 2, and dried under vacuum at 170 °C for 28 h.

$$CoCO_3 + 2HTFSA \rightarrow Co(TFSA)_2 + H_2O + CO_2 \quad [1]$$

$$Sm_2O_3 + 6HTFSA \rightarrow 2Sm(TFSA)_3 + 3H_2O \quad [2]$$

Electrochemical measurements were performed by using a single-compartment cell of three electrodes using a potentiostat (Hokuto Denko, HZ-7000) in an Ar-filled glove box (Miwa MFG, DBO-1K-SH, dew point < –75 °C). A glassy carbon (GC) disk (Tokai Carbon, GC-20SS, 0.71 cm^2) was used as a working electrode. A Co wire (Sanwa Kinzoku) was used as a counter electrode. A reference electrode was comprised of a silver wire (Sanwa Kinzoku) immersed in BMPTFSA containing 0.1 M $AgCF_3SO_3$ (Aldrich) and isolated by a porous glass (Vycor). The potential of this reference electrode indicated +0.44 V vs the ferrocene (Fc)/ferrocenium (Fc^+) couple. Potentiostatic cathodic reduction experiments were conducted using a double-compartment cell. A GC plate (Tokai Carbon, GC-20SS, 1.54 cm^2) was used as a substrate. The Co wire was placed in the counter electrode compartment which was separated with a poly-tetraflouroethylene made membrane filter (PTFE, Merck Millipore, Omnipore). The electrodeposits were washed with dehydrated monoglyme (G1) (Fujifilm Wako Pure Chemical Corp.) and characterized by a scanning electron microscope (SEM, Keyence, VE-9800) with an energy dispersive X-ray analyzer (EDX, Oxford Instruments, INCA-E250 × 3K) without exposure to air. After electrolysis, the deposits and the aggregates of the nanoparticles were also analyzed by X-ray diffractometer (XRD, Rigaku, Miniflex 600, Cu Kα, Ni filtered), Fourier transform infrared (FT-IR, Shimadzu, IRprestige-21) spectrometer with an attenuated total reflection apparatus (PIKE MIRacle™ ATR), and X-ray photoelectron spectrometer (XPS, Jeol, JPS-9010TR) using a transfer vessel for each analysis. The deposits and the electrolytes were collected on a copper grid (Oken Shoji) for transmission electron microscope (TEM), washed with G1 to remove the excess ionic liquids, and examined by TEM (FEI, TECNAI F20) combined with an EDX analyzer (Oxford Instruments, X-Mat 80T). A vacuum transfer holder (Gatan, VTST4006) was used for conducting the TEM analysis to avoid contact with air.

Results and Discussion

Electrochemical study of Co and Sm species at 25 °C.— Vacuum dried $Co(TFSA)_2$ and $Sm(TFSA)_3$ were dissolved in BMPTFSA at 25 °C to give a pink colored liquid. Figure 1 shows the cyclic voltammograms of a GC electrode in BMPTFSA containing (a) 30 mM $Co(TFSA)_2$, (b) 5 mM $Sm(TFSA)_3$, and (c) 30 mM $Co(TFSA)_2$ and 5 mM $Sm(TFSA)_3$ at 25 °C.

The ratio of the concentrations of Co and Sm species was determined based on the stoichiometry and the diffusion coefficients of the species. The concentration of Sm(III) was selected to be lower than that of Co(II) because of the difference in the diffusion coefficients of Co(II) and Sm(III) in BMPTFSA.[66,67] A cathodic current wave around –1.7 V and an anodic current wave around 0.3 V in Fig. 1a were ascribed to the reduction of Co(II) and the oxidation of Co deposited during the cathodic scan, respectively, as indicated by the reaction 3.

$$Co(II) + 2e^- \rightleftharpoons Co \quad [3]$$

The separation of 1.3 V (approx.) between the cathodic and anodic current wave indicated the large overpotential was required for the deposition of Co, as reported in the previous studies.[61,62] This overpotential might be caused by the inhibition of surface processes on the negatively polarized electrode, on which the bulky cations were accumulated in order to compensate the negative charge on the surface.[68] According to previous studies, the deposition of Co with very small grain sizes was observed at 25 °C.[66–68]

Figure 1b represents a cathodic and an anodic current wave for the reduction of Sm(III) to Sm(II) and the oxidation of Sm(II) generated during the prior cathodic scan to Sm(III), respectively, at 25 °C, according to the reaction 4.[69,70]

$$Sm(III) + e^- \rightleftharpoons Sm(II) \quad [4]$$

The anodic current wave corresponding to the Sm(II) was observed clearly because Sm(II) was stable in the time scale of the cyclic voltammetry with a scan rate of 10 mV s^{-1} at 25 °C. The reaction of Sm(III) to Sm(II) can be considered as electrochemically quasi-reversible or irreversible, as described in the previous study.[69] However, the anodic wave for the oxidation of Sm(II) was found

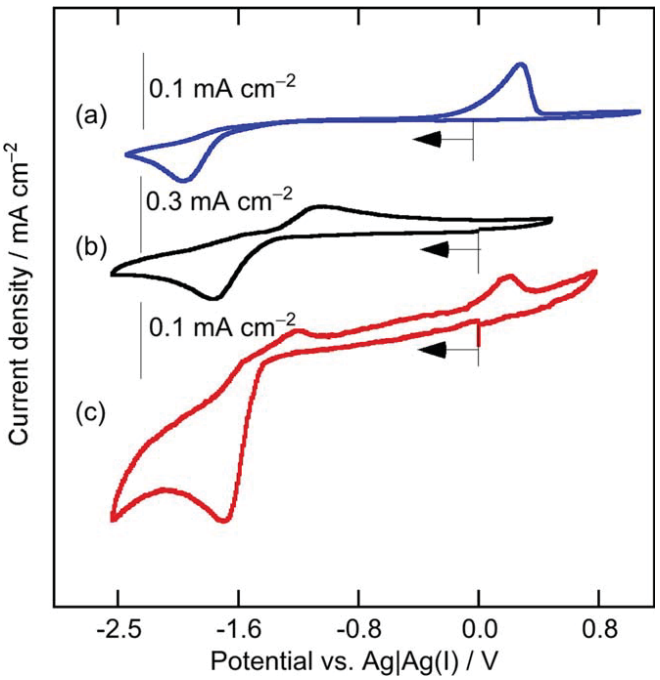

Figure 1. Cyclic voltammograms of a GC electrode (3 mmϕ) in BMPTFSA containing (a) 30 mM $Co(TFSA)_2$, (b) 5 mM $Sm(TFSA)_3$, and (c) 30 mM $Co(TFSA)_2$ and 5 mM $Sm(TFSA)_3$ at 25 °C. Scan rate: 10 mV s^{-1}.

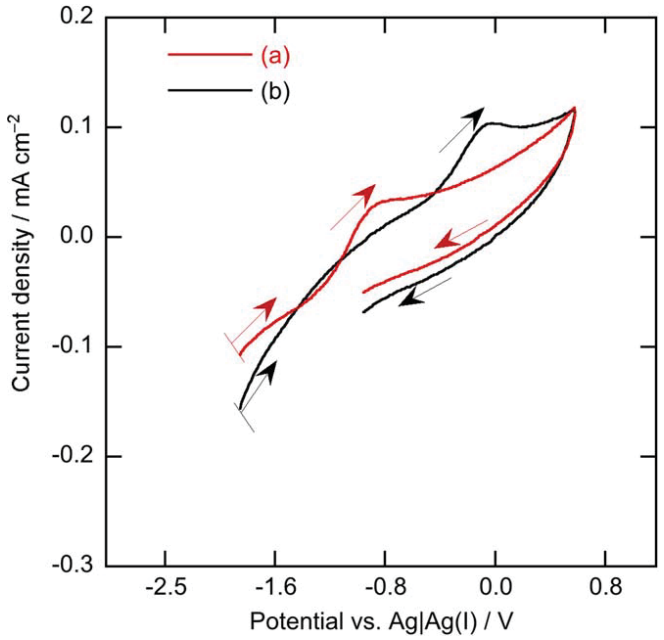

Figure 2. Cyclic voltammograms of a GC electrode (3 mmϕ) in BMPTFSA containing (a) 5 mM $Sm(TFSA)_3$ and (b) 30 mM $Co(TFSA)_2$ and 5 mM $Sm(TFSA)_3$ at 25 °C. The potential was held at –1.9 V for 60 s before the measurements. Scan rate: 10 mV s^{-1}.

to disappear with a low scan rate of 10 mV s^{-1} at 50 °C and 100 °C.[70,71] The disappearance of the oxidation wave of Sm(II) has been explained by a disproportionation reaction of Sm(II) to Sm(III) and Sm.[70,71] The stability of Sm(II) in BMPTFSA is known to decrease with elevating temperature.[70,71]

Figure 1c shows the cyclic voltammogram of a GC electrode in BMPTFSA containing 30 mM $Co(TFSA)_2$ and 5 mM $Sm(TFSA)_3$ at 25 °C. A large cathodic current wave observed around –1.4 V was considered to be assigned mainly to the reduction of Sm(III). The peak potential was slightly shifted to the more positive side as compared with that in BMPTFSA containing 5 mM $Sm(TFSA)_3$. Two anodic current waves around –1.3 V and 0.08 V were also found. The small wave around –1.3 V corresponding to the oxidation of Sm(II) disappeared at a scan rate of 5 mV s^{-1} even at 25 °C, suggesting Sm(II) was consumed in the presence of Co(II).

The electrode potential was held at –1.9 V for 60 s before each measurement in order to produce Sm(II) near the electrode surface. The cyclic voltammograms of a GC electrode in BMPTFSA containing 5 mM $Sm(TFSA)_3$ with and without 30 mM $Co(TFSA)_2$ at 25 °C are displayed in Fig. 2. An anodic wave corresponding to the oxidation of Sm(II) was observed around –1.0 V without Co(II). However, the anodic wave around –1.0 V was not observed in the presence of Co(II), as seen in Fig. 1c. An anodic current wave around –0.3 V can be assigned to the oxidation of Co deposited on the electrode surface at –1.9 V. These results suggested that the electrochemically generated Sm(II) is unstable in the presence of Co(II) even at 25 °C, and that Co(II) probably reacted with Sm(II).

Potentiostatic cathodic reduction at 25 °C.—Potentiostatic cathodic reduction on a GC electrode at –1.6 V was conducted in BMPTFSA containing 30 mM $Co(TFSA)_2$ and 5 mM $Sm(TFSA)_3$ at 25 °C. The color of the ionic liquid after the potentiostatic cathodic reduction changed from transparent pink to opaque gray. The deposits were analyzed by SEM, EDX, and XRD without exposure to air. Figure 3a shows the SEM image of the deposits obtained on the electrode. Co and Sm were detected in the deposits by EDX (Fig. 3b). The signals of F, S, and O indicated the presence of BMPTFSA in the deposits after washing with G1. No reflection corresponding to Co and/or Sm was found in the diffractogram of the deposits except for the diffraction peaks originated from GC. The similar results were also obtained by the potentiostatic cathodic reduction at –1.5, –1.7, –2.0, and –2.5 V at 25 °C.

Although it was considered that the reaction of Co(II) with the electrochemically generated Sm(II) might occur in the electrolyte, the granular deposits were obtained on the electrode. The deposits were rubbed off from the GC electrode, collected on a TEM grid, and examined by TEM. The TEM samples were exposed to air before TEM observation. The TEM image (Fig. 4) indicated the existence of nanoparticles with clear lattice fringes, implying the nanoparticles were crystalline. The inset represents the electron diffraction diagram obtained on the rectangular area, where the lattice fringes were observed on the nanoparticles. The interplanar spacings calculated from the observed spots were 0.243 and 0.210 nm, which could be ascribed to the (111) and (110) planes of metallic $SmCo_7$, 0.244 and 0.210 nm (ICDD: 01–079–8418), respectively.[4] Therefore, the deposits obtained on the GC electrode were identified as the aggregates of $SmCo_7$ nanoparticles. Due to the tiny size of the nanoparticles, no reflection was observed in the diffractogram.

The electrolyte after the potentiostatic cathodic reduction was also analyzed by TEM after exposing the sample to air. Figure 5a shows the TEM image of the nanoparticles found in the electrolyte. Lattice fringes were observed clearly in the nanoparticles. The electron diffraction diagram of the nanoparticles is shown in the insets of Fig. 5a. The interplanar spacings of these spots were estimated to be 0.244 and 0.210 nm, which could be assigned to the (111) and (110) planes of metallic $SmCo_7$.[4] The phase angle between the spots corresponding to (111) and (110) in the insets of Figs. 4 and 5a was 30.12°, which agrees with that calculated based on the crystal structure of $SmCo_7$. Similar $SmCo_7$ nanoparticles were found in the TEM sample without contact to air using the mentioned vacuum transfer holder, indicating the same characteristics of the nanoparticles were observed no matter if the samples were exposed to air, or not.

The formation of $SmCo_7$ was confirmed by the potentiostatic cathodic reduction in BMPTFSA containing $Co(TFSA)_2$ and $Sm(TFSA)_3$ at 25 °C. Since the disproportionation of Sm(II) to Sm and Sm(III) is unfavorable at 25 °C, Sm(II) was considered to reduce Co(II), as discussed above. In order to explain the formation of $SmCo_7$, Sm(II) has to act as both a reducing agent of Co(II) and source of Sm. The elemental reactions can be written as,

$$2Sm(II) + Co(II) \rightleftharpoons 2Sm(III) + Co \quad [5]$$

$$3Sm(II) + 7Co \rightleftharpoons 2Sm(III) + SmCo_7 \quad [6]$$

$$17Sm(II) + 7Co(II) \rightleftharpoons 16Sm(III) + SmCo_7 \quad [7]$$

Since Sm(II) is provided by electrochemical reduction of Sm(III) at –1.6 V, the reaction 5 can be regarded as the following reaction of the catalytic reaction (EC'), where Sm(III) is reproduced by the following reaction. Therefore, the oxidation of Sm(II) was not seen in Fig. 1c. Reaction 6 can be regarded as a disproportionation reaction for Sm although the one of the products is $SmCo_7$ alloy. This disproportionation reaction is considered to occur probably because of the formation of $SmCo_7$ in the presence of elementary Co is thermodynamically more favorable than that of Sm. In addition, the reaction 6 is also regarded as the following reaction of the catalytic reaction because Sm(III) is reproduced. Thus, the large irreversible cathodic reduction wave in Fig. 1c can be explained by these following reactions occurring simultaneously. The total electrode reaction at –1.6 V can be represented as follows.

$$Sm(III) + 17\,e^- + 7Co(II) \rightleftharpoons SmCo_7 \quad [8]$$

Reaction of Sm(II) with Co(II) at 25 °C.—In order to verify the above hypothesis on the formation of $SmCo_7$, the ionic liquid containing Sm(II) was prepared by bulk electrolysis and mixed with

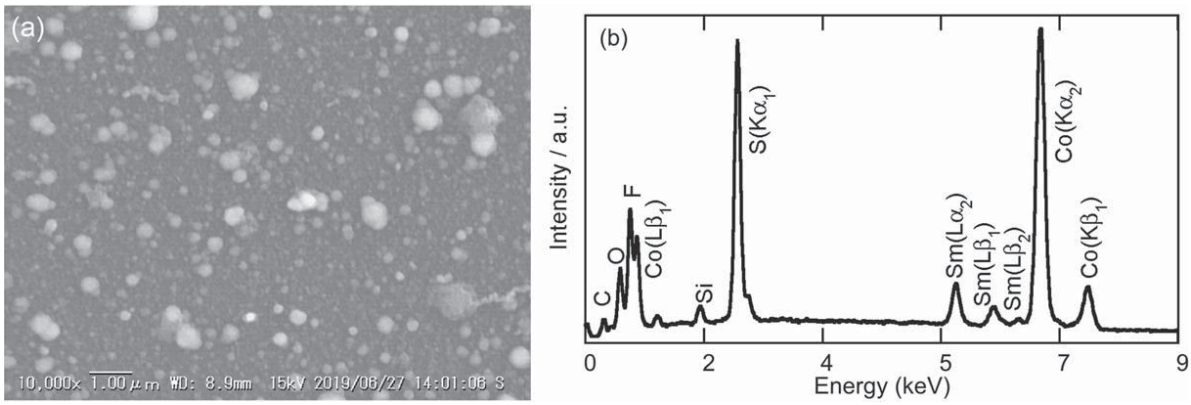

Figure 3. (a) SEM image and (b) EDX spectrum of the deposits obtained on a GC electrode after potentiostatic cathodic reduction at –1.6 V in BMPTFSA containing 30 mM $Co(TFSA)_2$ and 5 mM $Sm(TFSA)_3$. Temperature: 25 °C. Electric charge: 1.2 C.

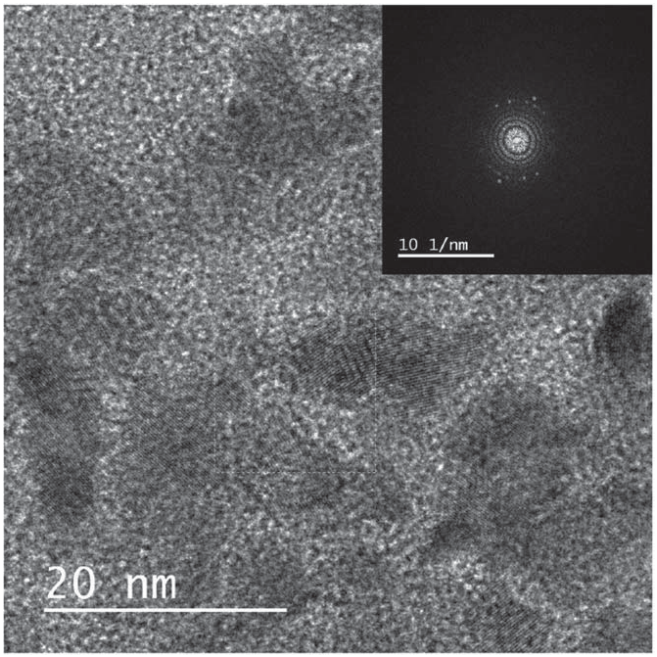

Figure 4. TEM image of the deposits rubbed from a GC electrode after potentiostatic cathodic reduction at –1.6 V in BMPTFSA containing 30 mM $Co(TFSA)_2$ and 5 mM $Sm(TFSA)_3$. Temperature: 25 °C. Electric charge: 1.2 C. The inset displays the electron diffraction diagram obtained on the rectangular area.

that containing Co(II). Figure 6 shows the cyclic voltammograms of a carbon cloth electrode in BMPTFSA containing 10 mM $Sm(TFSA)_3$ before and after bulk electrolysis. The cathodic and anodic current peak were observed before the bulk electrolysis in the same way as observed in Fig. 1b. After bulk electrolysis with the electric charge of 1 C for 3 ml of BMPTFSA containing 10 mM $Sm(TFSA)_3$, the electrolyte turned from colorless to light yellow. No nanoparticles were found in the electrolyte after the bulk electrolysis, denoting Sm nanoparticles were not produced by the disproportionation reaction at 25 °C. An anodic current peak corresponding to the oxidation of Sm(II) was observed after the bulk electrolysis as shown in Fig. 6.

After the bulk electrolysis, BMPTFSA containing Sm(II) was mixed with that containing 30 mM $Co(TFSA)_2$. The mixture was kept in Ar-atmosphere overnight. The color of the mixture slightly changed to pale gray. Formation of nanoparticles was confirmed in the mixture by TEM (Fig. 7a). The EDX spectrum of the nanoparticles showed the presence of Co and Sm in addition to the elements from the ionic liquid. Two diffraction spots found in the electron diffraction diagram of the nanoparticles (inset of Fig. 7a) could be identified as (111) and (110) planes of $SmCo_7$, indicating $SmCo_7$ was formed according to the reaction 7, which includes the disproportionation reaction of Sm(II), as discussed above. Therefore, the electrode reaction 8 is considered to be feasible in BMPTFSA at 25 °C.

IR spectroscopy and XPS analysis of the Co-Sm nanoparticles.—As F, S, and O were detected in the EDX spectra (Figs. 3b, 5b, and 7b) BMP^+ and/or $TFSA^-$ might be present and protect the

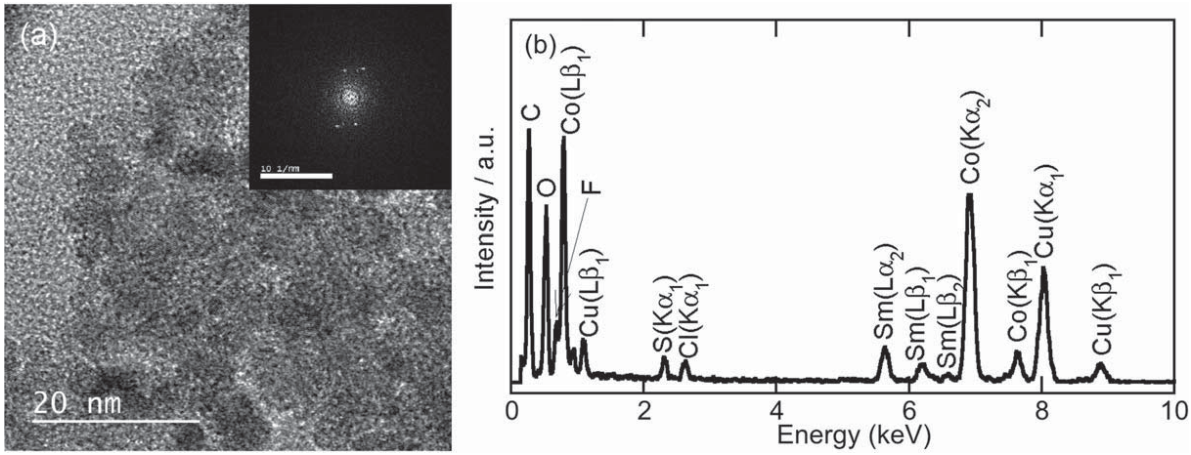

Figure 5. (a) TEM image and (b) EDX spectrum of the nanoparticles dispersed in BMPTFSA after potentiostatic cathodic reduction on a GC electrode at –1.6 V in BMPTFSA containing 30 mM $Co(TFSA)_2$ and 5 mM $Sm(TFSA)_3$. Temperature: 25 °C. Electric charge: 1.2 C. The inset displays the electron diffraction diagram of the nanoparticles.

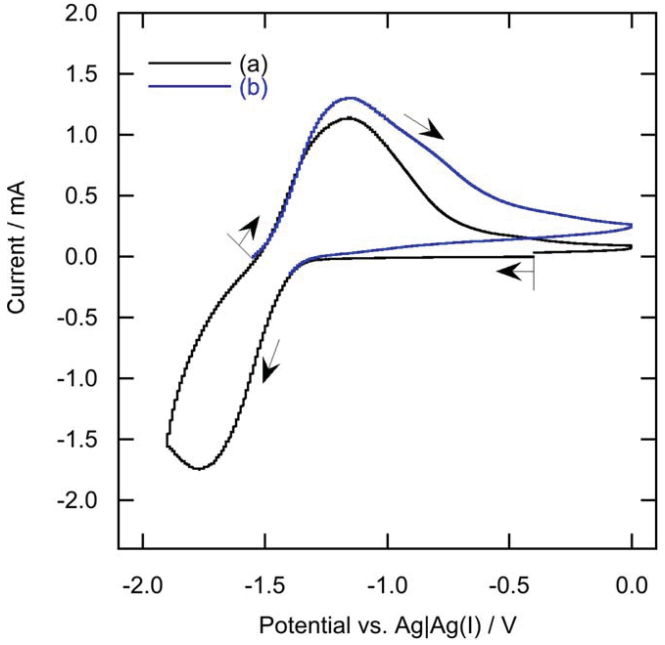

Figure 6. Cyclic voltammograms of a carbon cloth electrode (a) before and (b) after bulk electrolysis at −1.6 V in BMPTFSA containing 10 mM $Sm(TFSA)_3$. Temperature: 25 °C. Scan rate: 10 mV s^{-1}.

Co-Sm nanoparticles. Figure 8 shows the ATR-FT-IR spectrum of the aggregates of $SmCo_7$ nanoparticles prepared by the reaction 8. The nanoparticles were precipitated by the addition of G1 and centrifugation. The absorption peaks observed in the FT-IR spectrum were assigned to $TFSA^-$.[72–74] Although no peak assignable to BMP^+ could be observed in the range of wavenumber, $SmCo_7$ nanoparticles were suggested to be covered with BMPTFSA. The same sample was also examined by XPS. However, no peak corresponding to Co and Sm was detected probably due to a tiny amount of the sample, while the signals corresponding to F, S, and O derived from $TFSA^-$ were detected.

Since $SmCo_7$ is ferromagnetic, $SmCo_7$ nanoparticles are expected to be collected by a magnet. Thus, potentiostatic cathodic reduction on a GC electrode attached with a NdFeB magnet (6 mm in diameter) on its back was conducted in BMPTFSA containing 30 mM $Co(TFSA)_2$ and 5 mM $Sm(TFSA)_3$ at −1.6 V. A significant amount of deposits were obtained on the electrode after the potentiostatic cathodic reduction probably because ferromagnetic $SmCo_7$ nanoparticles were attracted and attached to the electrode

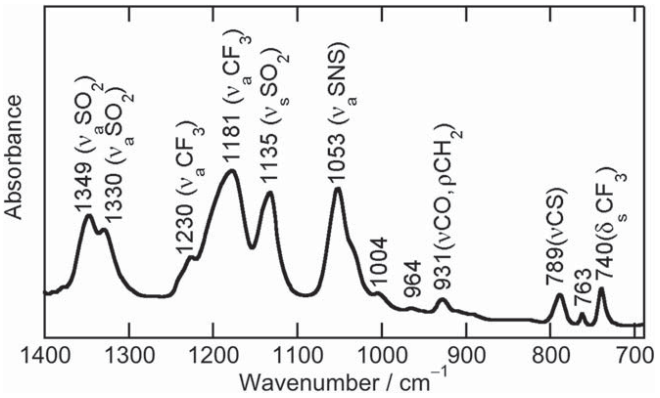

Figure 8. ATR-FT-IR spectrum of the aggregates of the nanoparticles collected after potentiostatic cathodic reduction at −1.6 V in BMPTFSA containing 30 mM $Co(TFSA)_2$ and 5 mM $Sm(TFSA)_3$. Temperature: 25 °C. Electric charge: 1.2 C.

surface by the permanent magnet. Figure 9 shows the SEM images of the deposits obtained after the potentiostatic cathodic reduction. Granular deposits were found on the edge of the electrode, as shown in Fig. 9a, while nanowire-shaped deposits were observed on the center of the GC, as shown in Fig. 9b. The nanowire-shaped deposits might be formed by the magnetic field produced from the magnet. Co and Sm were detected in the nanowires by EDX. The deposits were also found to be composed of $SmCo_7$ nanoparticles by TEM. The mechanism of the formation of $SmCo_7$ nanowires is the topic of ongoing investigations.

XPS spectra of the collected deposits after Ar^+ etching are shown in Fig. 10. A peak corresponding to Co $2p_{3/2}$ was clearly observed at 781.0 eV, which was slightly higher than that for metallic Co (778.7 eV) and CoO (779.7 eV).[75–78] In the case of Sm $3d_{5/2}$, a peak was observed at 1084.0 eV, which was also slightly higher than metallic Sm (1081.0 eV) and Sm_2O_3 (1083.5 eV).[42,45] Since the binding energy for contaminated carbon was identical to the literature value, the slight shift of the binding energies of Co and Sm indicated formation of the intermetallic compound of $SmCo_7$.[42,79–82] In addition, F and S assignable to $TFSA^-$ were detected by XPS, verifying the existence of $TFSA^-$ in the sample.[82,83] The binding energy of the F 1 s peak at 689.5 eV was slightly higher than that observed for the ionic liquids, suggesting the $TFSA^-$ in the sample interacts with the nanoparticles. The F 1 s peak around 685.5 eV was assigned to the decomposed $TFSA^-$ by Ar^+ etching.[82] Therefore, the stability of $SmCo_7$ nanoparticles in air might be caused by a protecting shell of BMPTFSA.[84–90]

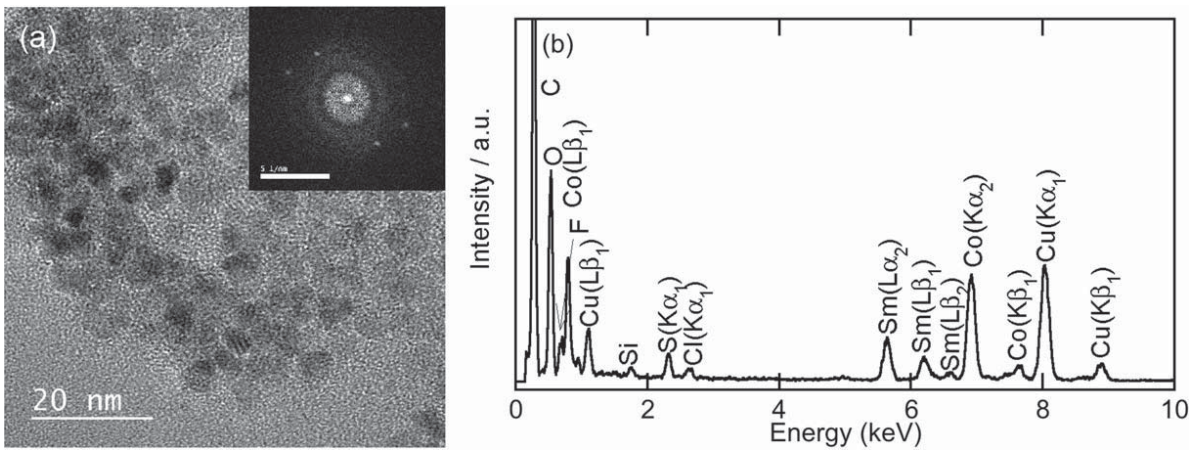

Figure 7. (a) TEM image and (b) EDX spectrum of the nanoparticles dispersed in BMPTFSA after mixing Sm(II)/BMPTFSA and Co(II)/BMPTFSA at 25 °C. for 16 h. The inset displays the electron diffraction diagram of the nanoparticles.

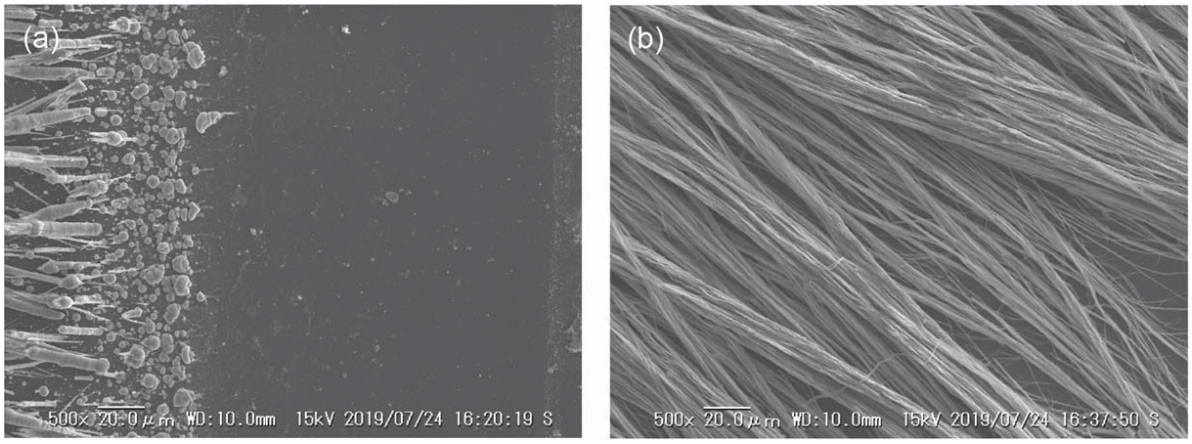

Figure 9. SEM images of the (a) edge and (b) center part of the GC electrode with a NdFeB magnet after potentiostatic cathodic reduction at –1.6 V in BMPTFSA containing 30 mM $Co(TFSA)_2$ and 5 mM $Sm(TFSA)_3$. Temperature: 25 °C. Electric charge: 1.2 C.

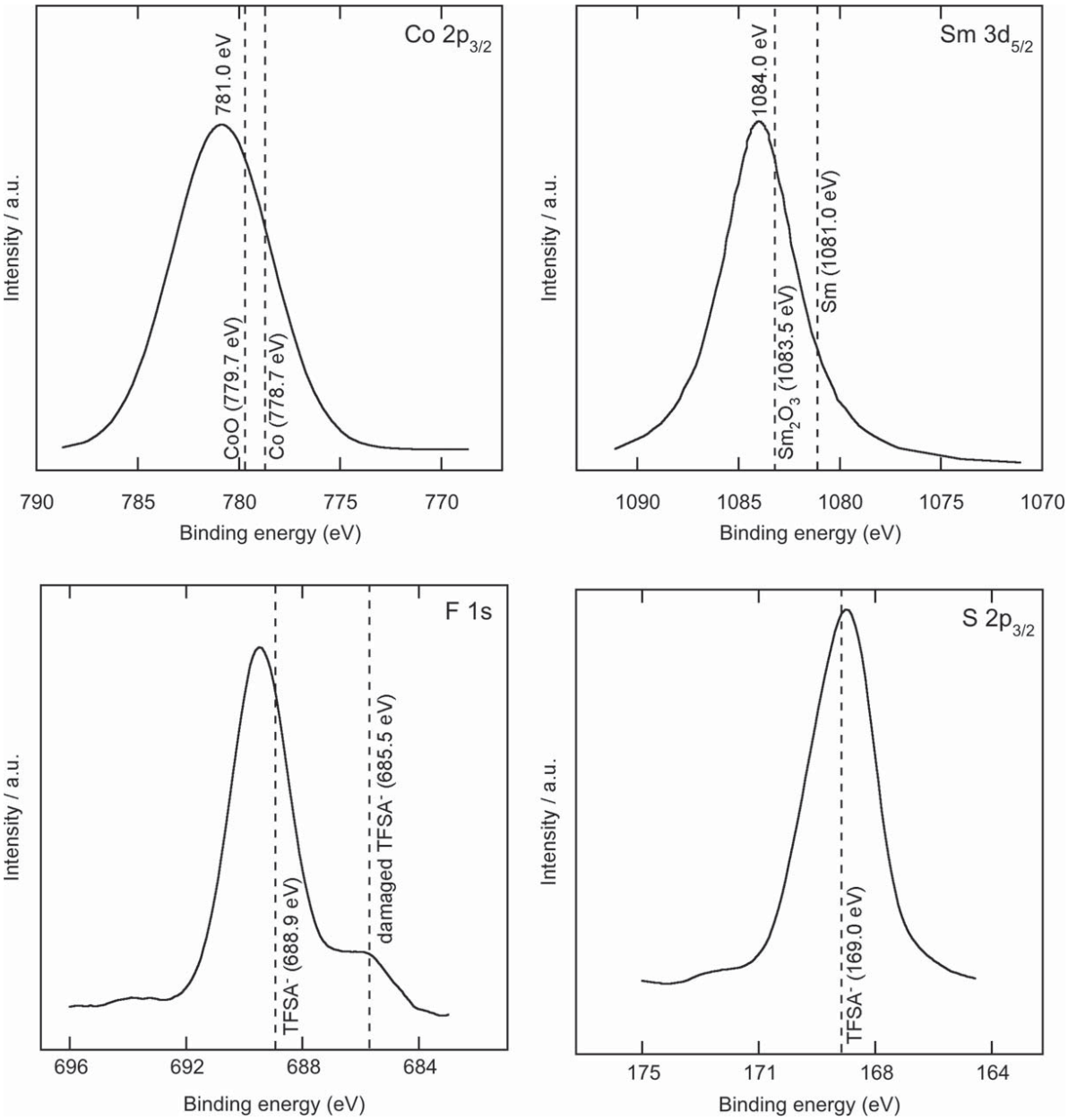

Figure 10. XPS spectra of the deposits obtained on a GC electrode with a NdFeB magnet after potentiostatic cathodic reduction at –1.6 V in BMPTFSA containing 30 mM $Co(TFSA)_2$ and 5 mM $Sm(TFSA)_3$. Temperature: 25 °C. Electric charge: 1.2 C.

Conclusions

The irreversible cathodic peak was observed in the cyclic voltammogram of a GC electrode in BMPTFSA containing Sm(II) in the presence of Co(II) at 25 °C, is probably due to the following reactions corresponding to reduction of Co(II) and the disproportionation reaction of Sm(II). Electrochemical preparation of $SmCo_7$ nanoparticles was possible in BMPTFSA containing $Co(TFSA)_2$ and $Sm(TFSA)_3$ at 25 °C probably because the disproportionation reaction of Sm(II) was promoted by the formation of $SmCo_7$ nanoparticle, which is more favorable than Sm nanoparticles at 25 °C. This reaction can be called "alloying-assisted disproportionation reaction." Formation of $SmCo_7$ was also confirmed by the reaction of Sm(II) with Co(II) in BMPTFSA, supporting the mechanism of electrochemical formation of $SmCo_7$. The $SmCo_7$ nanoparticles were stable in air because FT-IR, EDX, and XPS showed the existence of BMPTFSA, which might act as a protective layer against the oxidation by oxygen and moisture. However, the protective layer might prevent the crystal growth of the deposits in this system. Furthermore, it was found that the nanowire-shaped electrodeposits $SmCo_7$ were obtained by attaching a magnet behind the GC electrode during potentiostatic cathodic reduction. The mechanism of the formation of nanowires is still unknown. Therefore, BMPTFSA is considered to be used for the preparation of various magnetic nanoparticles and nanowires at a lower temperature.

Acknowledgments

The author (MM) kindly acknowledges the financial support provided by the Keio Leading-edge Laboratory of Science and Technology (KLL) and Ministry of Education, Culture, Sports, Science and Technology (MEXT), Japan.

ORCID

Marjanul Manjum https://orcid.org/0000-0002-3678-9715
Nobuyuki Serizawa https://orcid.org/0000-0002-8939-272X
Andreas Bund https://orcid.org/0000-0001-9837-2408
Yasushi Katayama https://orcid.org/0000-0002-4057-8398

References

1. T. Hyeon, *Chem. Commun.*, 927 (2003).
2. G.-R. Li, Z.-S. Zhang, C.-Y. Su, and Y.-X. Tong, *J. Phys. Chem. C*, **113**, 1227 (2009).
3. S. Yagi, M. Kawamori, and E. Matsubara, *J. Electrochem. Soc.*, **157**, E92 (2010).
4. Z. X. Zhang, X. Y. Song, W. W. Xu, M. Seyring, and M. Rettenmayr, *Scr. Mater.*, **62**, 594 (2010).
5. L. Peng, X. Tu, L. Li, and R. Wang, *J. Nanoelectron. Optoelectron.*, **8**, 458 (2013).
6. S. Sun, C. B. Murray, D. Weller, L. Folks, and A. Moser, *Science*, **287**, 2000 (1989).
7. K. J. Strnat, *Proc. IEEE*, **78**, 923 (1990).
8. J. Chen and L. Rissing, *J. Appl. Phys.*, **109**, 07A766 (2011).
9. A. Morisako, I. Kato, S. Takei, and X. Liu, *J. Magn. Magn. Mater.*, **303**, e274 (2006).
10. L. Peng, H. Zhang, Q. Yang, Y. Li, Y. Song, and J. Shen, *J. Appl. Phys.*, **105**, 063915 (2009).
11. Y. Q. Guo, W. Li, J. Luo, W. C. Feng, and J. K. Liang, *J. Magn. Magn. Mater.*, **303**, e367 (2006).
12. J. Lee, T.-Y. Hwang, M. K. Kang, H.-B. Cho, J. Kim, N. V. Myung, and Y.-H. Choa, *Front Chem.*, **6**, 18 (2018).
13. L. T. Roling, T. S. Choksi, and F. A.- Pedersen, *Nanoscale*, **11**, 4438 (2019).
14. M. Seyring, X. Song, Z. Zhang, and M. Rettenmayr, *Nanoscale*, **7**, 12126 (2015).
15. H. Hegde, S. U. Jen, K. Chen, and F. J. Cadieu, *J. Appl. Phys.*, **73**, 5926 (1993).
16. H.-C. Yu, J.-Q. Li, Y.-Q. Bei, Y.-Q. Zhou, J. Zhang, W.-Y. Zhang, and B.-G. Shen, *J. Electron Microsc.*, **53**, 37 (2004).
17. H. Ohno (ed.), *Electrochemical aspects of ionic liquids* (John Wiley & Sons, Inc., Hoboken, NJ) 2nd ed. (2005).
18. M. Siebels et al., *Beilstein J. Nanotechnol.*, **9**, 1881 (2018).
19. F. Endres and S. Z. E. Abedin, *Phys. Chem. Chem. Phys.*, **8**, 2101 (2006).
20. A. P. Abbott and K. J. McKenzie, *Phys. Chem. Chem. Phys.*, **8**, 4265 (2006).
21. J. DuPont and J. D. Scholten, *Chem. Soc. Rev.*, **39**, 1780 (2010).
22. T. Torimoto, K. Okazaki, T. Kiyama, K. Hirahara, N. Tanaka, and S. Kuwabata, *Appl. Phys. Lett.*, **89**, 243117 (2006).
23. T. Tsuda, S. Seino, and S. Kuwabata, *Chem. Commun.*, 6792 (2009).
24. T. Tsuda, K. Yoshii, T. Torimoto, and S. Kuwabata, *J. Power Sources*, **195**, 5980 (2010).
25. M. Brettholle, O. Hofft, L. K. Larhofer, S. Mathes, W. Maus-Friedrichs, S. Z. E. Abedin, S. Krischok, J. Janek, and F. Endres, *Phys. Chem. Chem. Phys.*, **12**, 1759 (2010).
26. A. Imanishi, S. Gonsui, T. Tsuda, S. Kuwabata, and K. Fukui, *Phys. Chem. Chem. Phys.*, **13**, 14823 (2011).
27. H. Wender, M. L. Andreazza, R. R. B. Correia, S. R. Teixeira, and J. DuPont, *Nanoscale*, **3**, 1240 (2011).
28. F. Endres, D. R. MacFarlane, and A. P. Abbott, *Electrodeposition from ionic liquids* (Wiley-VCH Verlag GmbH & Co. KGaA, Weinheim) (2008).
29. J. S. Wilkes, *Green Chem.*, **4**, 73 (2002).
30. T. Torimoto, T. Tsuda, K. Okazaki, and S. Kuwabata, *Adv. Mater.*, **22**, 1196 (2010).
31. L. S. Ott, M. L. Cline, M. Deetlefs, K. R. Seddon, and R. G. Finke, *J. Am. Chem. Soc.*, **127**, 5758 (2005).
32. N. Serizawa, Y. Katayama, and T. Miura, *J. Electrochem. Soc.*, **156**, D503 (2009).
33. M. Yamagata, N. Tachikawa, Y. Katayama, and T. Miura, *Electrochemistry*, **73**, 564 (2005).
34. Y.-L. Zhu, Y. Katayama, and T. Miura, *Electrochem. Solid-State Lett.*, **14**, D110 (2011).
35. Y. Katayama, R. Fukui, and T. Miura, *Electrochemistry*, **81**, 532 (2013).
36. Y. Katayama, Y. Toshimitsu, and T. Miura, *J. Electrochem. Soc.*, **160**, H219 (2013).
37. Y. Bando, Y. Katayama, and T. Miura, *Electrochim. Acta*, **53**, 87 (2007).
38. Y. Katayama, Y. Bando, and T. Miura, *Trans. Inst. Met. Finish.*, **86**, 205 (2008).
39. S. Saha, T. Taguchi, N. Tachikawa, K. Yoshii, and Y. Katayama, *Electrochim. Acta*, **183**, 42 (2015).
40. J. Gong and E. J. Podlaha, *Electrochem. Solid State Lett.*, **3**, 422 (2000).
41. X.-F. Long, G.-H. Guo, X.-H. Li, Q.-L. Xia, and J.-F. Zhang, *Thin Solid Films*, **548**, 259 (2013).
42. E. Herrera, J. Riva, G. Pozo-López, A. Condó, S. E. Urreta, and L. M. Fabietti, *J. Electrochem. Soc.*, **166**, D460 (2019).
43. J. C. Wei, M. Schwartz, and K. Nobe, *J. Electrochem. Soc.*, **155**, D660 (2008).
44. J. C. Wei, M. Schwartz, and K. Nobe, *ECS Trans.*, **50**, 79 (2013).
45. Y. Sato, H. Ishida, K. Kobayakawa, and Y. Abe, *Chem. Lett.*, **19**, 1471 (1990).
46. Q.-W. Chu, J. Liang, and J.-C. Hao, *Electrochim. Acta*, **115**, 499 (2014).
47. G. Panzeri and L. Magagnin, *ECS Trans.*, **75**, 31 (2016).
48. G. Panzeri, M. Tresoldi, C. Rinaldi, and L. Magagnin, *J. Electrochem. Soc.*, **164**, D930 (2017).
49. P. Liu, Y. P. Du, Q. Q. Yang, Y. X. Tong, and G. A. Hope, *J. Electrochem. Soc.*, **153**, C57 (2006).
50. L. Xiaohua, L. Zheng, O. Martina, and B. Koen, *ACS Sustain. Chem. Eng.*, **7**, 2578 (2019).
51. E. Gomez, P. Cojocaru, L. Magagnin, and E. Valles, *J. Electroanal. Chem.*, **658**, 18 (2011).
52. P. Cojocaru, L. Magagnin, E. Gomez, and E. Vallés, *Mat. Lett.*, **65**, 3597 (2011).
53. E. Gomez, E. Valles, P. Cojocaru., A. Raygani, and L. Magagnin, *ECS Trans.*, **41**, 3 (2012).
54. A. I. Bhatt, I. May, V. A. Volkovich, D. Collison, M. Helliwell, I. B. Polovov, and R. G. Lewin, *Inorg. Chem.*, **44**, 4934 (2005).
55. A. Ispas, M. Buschbeck, S. Pitula, A. Mudring, M. Uhlemann, A. Bund, and F. Endres, *ECS Trans.*, **16**, 119 (2009).
56. A. I. Bhatt, I. May, V. A. Volkovich, M. E. Hetherington, B. Lewin, R. C. Thied, and N. Ertok, *J. Chem. Soc., Dalton Trans.*, 4532 (2002).
57. C. J. Rao, K. A. Venkatesan, K. Nagarajan, T. G. Srinivasan, and P. R. V. Rao, *J. Nucl. Mater.*, **399**, 81 (2010).
58. A. Kurachi, M. Matsumiya, K. Tsunashima, and S. Kodama, *J. Appl. Electrochem.*, **42**, 961 (2012).
59. M. Matsumiya, Y. Kikuchi, T. Yamada, and S. Kawakami, *Sep. Purif. Technol.*, **130**, 91 (2014).
60. C. J. Rao, K. A. Venkatesan, K. Nagarajan, T. G. Srinivasan, and P. R. V. Rao, *J. Electrochim. Acta*, **54**, 4718 (2009).
61. C. L. Hussey and L.-H. Chou, *J. Inorg. Chem.*, **53**, 5750 (2014).
62. Y. Chen, H. Wang, and B. Li, *RSC Adv.*, **5**, 39620 (2015).
63. Y. Cui, Y. Hua, and Y. Lin, *J. Chongqing Univ. (Engl. Ed.)*, **9**, 167 (2010), https://pdfs.semanticscholar.org/82a0/250f27df8d1c968d40b258dec85fb5577ac3.pdf.
64. X. Yang, L. He, S. Qin, G.-H. Tao, M. Huang, and Y. LV, *PLoS One*, **9**, e95832 (2014).
65. C. J. Rao, K. A. Venkatesan, K. Nagarajan, T. G. Srinivasan, and P. R. V. Rao, *J. Nucl. Mater.*, **399**, 81 (2010).
66. R. Fukui, Y. Katayama, and T. Miura, *Electrochemistry*, **73**, 567 (2005).
67. Y. Katayama, R. Fukui, and T. Miura, *J. Electrochem. Soc.*, **154**, D534 (2007).
68. R. Fukui, Y. Katayama, and T. Miura, *Electrochim. Acta*, **56**, 1190 (2011).
69. M. Yamagata, Y. Katayama, and T. Miura, *J. Electrochem. Soc.*, **153**, E5 (2006).
70. M. Manjum, N. Tachikawa, N. Serizawa, and Y. Katayama, *J. Electrochem. Soc.*, **166**, D483 (2019).
71. Y.-F. Pan and C. L. Hussey, *Inorg. Chem.*, **52**, 3241 (2013).
72. M. Herstedt, M. Smirnov, P. Johansson, M. Chami, J. Grondin, L. Servant, and J. C. Lassegues, *J. Raman Spectrosc.*, **36**, 762 (2005).
73. I. Rey, P. Johansson, J. Lindgren, J. C. Lassegues, J. Grondin, and L. Servant, *J. Phys. Chem. A*, **102**, 3249 (1998).
74. N. Mozhzhukhina, A. Y. Tesio, L. P. M. D. Leo, and E. J. Calvo, *J. Electrochem. Soc.*, **164**, A518 (2017).
75. Y. Okamoto, T. Shimokawa, T. Imanaka, and S. Teranishi, *J. Catal.*, **57**, 153 (1979).
76. J. Jansson, A. E. C. Palmqvist, E. Fridell, M. Skoglundh, L. Osterlund, P. Thormahlen, and V. Langer, *J. Catal.*, **211**, 387 (2002).

77. M. C. Biesinger, B. P. Payne, A. P. Grosvenor, L. W. M. Lau, A. R. Gerson, and R. S. C. Smart, *Appl. Surf. Sci.*, **257**, 2717 (2011).
78. T.-D. Nguyen, D. Mrabet, and T.-O. DoIkeda, *J. Phys. Chem. C*, **112**, 15226 (2008).
79. Y. Wei, H. Fan, and R. Wang, *App. Surf. Sci.*, **459**, 63 (2018).
80. Y. H. Liu et al., *J. All. Comp.*, **772**, 978 (2019).
81. C. C. Naik and A. V. Salker, *Mater. Res. Express*, **6**, 066112 (2019).
82. S. Men, K. R. J. Lovelock, and P. Licence, *Phys. Chem. Chem. Phys.*, **13**, 15244 (2011).
83. I. Shterenberg, M. Salama, Y. Gofer, and D. Aurbach, *J. Phys. Chem. C*, **121**, 3744 (2017).
84. F. H. Ellinger and W. H. Zachariasen, *J. Am. Chem. Soc.*, **75**, 5650 (1953).
85. Y. Katayama, T. Endo, T. Miura, and K. Toshima, *J. Electrochem. Soc.*, **160**, D423 (2013).
86. F. D. Lewis, G. D. Salvi, D. R. Kanis, and M. A. Ratner, *Inorg. Chem.*, **32**, 1251 (1993).
87. H. Sato, S. Saha, N. Tachikawa, K. Yoshii, N. Serizawa, and Y. Katayama, *Electrochemistry*, **86**, 57 (2018).
88. Y. Katayama, Y. Oshino, N. Ichihashi, N. Tachikawa, K. Yoshii, and K. Toshima, *Electrochim. Acta*, **183**, 37 (2015).
89. R. Fukui, Y. Katayama, and T. Miura, *J. Electrochem. Soc.*, **158**, D567 (2011).
90. N. G. Gheorghe, G. A. Lungu, M. A. Husanu, R. M. Costescu, D. Macovei, and C. M. Teodorescu, *App. Surf. Sci.*, **267**, 106 (2013).